View metadata, citation and similar papers at core.ac.uk
brought to you by CORE
provided by The Australian National University

Random-Phase Beamforming for Initial Access in Millimeter-Wave Cellular Networks

Zohair Abu-Shaban*, Henk Wymeersch†, Xiangyun Zhou*, Gonzalo Seco-Granados‡, Thushara Abhayapala*
*The Australian National University, Australia.
Email: {zohair.abushaban, xiangyun.zhou, thushara.abhayapala}@anu.edu.au
†Chalmers University of Technology, Sweden.
Email: henkw@chalmers.se
‡Universitat Autònoma de Barcelona, Spain.
Email: gonzalo.seco@uab.es

***Abstract*—The utilization of the millimeter-wave frequency band (mm-wave) in the fifth generation (5G) of mobile communication is a highly-debated current topic. Mm-wave MIMO systems will use arrays with large number of antennas at the transmitter and the receiver, implemented on a relatively small area. With the inherent high directivity of these arrays, algorithms to help the user equipment find the base station and establish a communication link should be carefully designed. Towards that, we examine two beamforming schemes, namely, random-phase beamforming (RPBF) and directional beamforming (DBF), and test their impact on the Cramér-Rao lower bounds (CRB) of jointly estimating the direction-of-arrival, direction-of-departure, time-of-arrival, and the complex channel gain, under the line-of-sight channel model. The results show that the application of RPBF is more appropriate in the considered scenario as it attains a lower CRB with fewer beams compared to DBF.**

I. Introduction

One of the enabling technologies of the fifth generation of mobile networks (5G) is the millimeter-wave technology (mm-wave) [1], [2]. Mm-waves allow packing high number of antennas in a relatively small area due to their small wavelengths – from 1 mm to 1 cm. In addition, the massively available spectrum of mm-wave would easily enable the transmission with extremely high data rates [3]. These two reasons reinforce the role that the mm-wave technology can play in 5G.

Due to the special characteristics of the mm-wave channel, directional transmission with large-size arrays, at both the transmitter and the receiver, is going to be utilized [4]. However, when initiating a communication link, this high directionality is an issue for a user equipment (UE) trying to find the base station (BS), and vise versa, especially that omni-directional transmission with antenna arrays is a challenge itself [5], [6].

The mm-wave initial access (IA) techniques with analog beamforming were reviewed in [7]. The three approaches compared therein include two direction-based methods, namely exhaustive search and iterative search. The third method is GPS-assisted algorithm. The disadvantage of these approaches is mainly the delay of finding the proper transmission direction.

In contrast to the directional methods covered in [7], we focus on random beamforming. The concept of random beamforming is not new per-se. Randomly-directional beamforming is a method of opportunistic beamforming that was investigated in [8], [9] for mm-wave receivers. Under this scheme, the BS generates narrow beams with random directions and select the user with the highest signal-to-noise ratio. On the other hand, optimization-based random beamforming in [6] optimizes the beamforming weights so that the resulting beam pattern is omni-directional. The work therein focused on conventional multiple-input-multiple-output (MIMO) systems in the microwave band. Despite the advantage of omni-directional coverage in the AI phase, the cost function is complex and, for a high number of antennas, it is only solvable numerically. Another random beamforming investigated under conventional MIMO is the unitary beamforming, whereby the beamforming matrix is obtained by the singular value decomposition of the channel matrix, see for example [10]. This is not applicable in an IA scenario since the channel is unknown at that phase.

The Cramér-Rao lower bounds (CRB) of a line-of-sight (LOS) mm-wave channel parameters were previously studied in [11]. Therein, the CRBs were provided as a function of the Fisher information matrix (FIM), whose entries were given by high level expressions and are valid for uniform linear arrays (ULA) with *directional beamforming* (DBF).

In this paper, we investigate a random beamforming scheme, referred to as *random-phase beamforming* (RPBF). Under this scheme, the beamforming vector is generated as a vector of complex exponentials with independent and identically distributed (i.i.d.) random phases. This scheme is used in [12] to initiate an iterative beamforming scheme which assumes full channel knowledge, and in [13], which assumes the direction-of-departure (DOD) to be known. However, these two assumptions are not used in this paper. We look into the IA problem for a LOS mm-wave channel. Towards that, we study the effect of beamforming on the estimation bounds of the direction-of-arrival (DOA), DOD, time-of-arrival (TOA), and the complex channel gain. The current paper presents the CRB expressions for an *arbitrary array geometry*. Moreover, as a special case, we obtain expressions of CRB, using ULA, simpler than those in [11]. Although mm-wave may apply different array geometries, ULA is the standard array structure that is usually used to get initial insights. Finally, we investigate and assess the RPBF and DBF in terms of the CRB, as a function of the number of transmit antennas, receive antenna and transmit beams.

II. Problem Formulation

Consider the scenario illustrated in Fig. 1, where the receiver and the transmitter are equipped with arrays of N_R and N_T

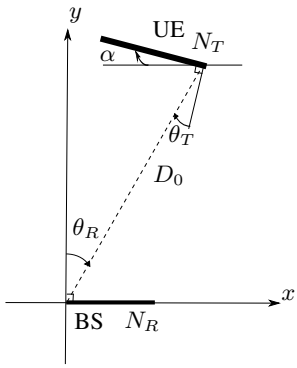

Fig. 1. A schematic diagram of the considered scenario. Angles are positive clockwise. D_0 is the transmitter-receiver separation distance.

antennas, respectively. Without loss of generality, we consider the uplink and assume that the BS and UE are located in the same plane. Consequently, we consider a 2D approach. Moreover, similar to [11], we assume that the UE and BS communicate via a LOS path only. In fact, the effect of NLOS links is limited, since 1) the path loss exponent is much higher than the case of LOS, and 2) the absorption loss is high and results in weak reflections. These factors cause NLOS to have 20 dB less power than LOS at 38 GHz [14]. Furthermore, we assume that the transmit antenna array is rotated by an unknown angle α. Finally, we assume that the arrays are narrow-band, i.e., the signal traverses the arrays apertures, both at the transmitter and the receiver, within a fraction of a symbol duration. That is $A_{\max} = c\mu T_s$, where $A_{\max}$ is the maximum array aperture, $c = 3 \times 10^8$ m/s is the speed of light, T_s is the symbol duration, and $0 < \mu < 1$. Based on the above assumptions, the channel matrix is modeled by [4]

$$\mathbf{H} \triangleq \sqrt{N_R N_T}\beta \mathbf{a}_R(\theta_R)\mathbf{a}_T^H(\theta_T) \in \mathbb{C}^{N_R \times N_T},$$

where $\beta = \beta_R + j\beta_I \in \mathbb{C}$ is the complex channel gain, θ_R is the DOA, and θ_T is the DOD. Under mm-wave channel, DOD is crucial in beamforming, since the knowledge of DOD would enable more efficient beamforming[12]. Moreover, $\mathbf{a}_R(\theta_R) \in \mathbb{C}^{N_R}$ is the receiver array response vector, and $\mathbf{a}_T(\theta_T) \in \mathbb{C}^{N_T}$ is the transmitter array steering vector. As an example, for the particular case of ULA, these two vector are given by (18) and (17). For notation simplicity, we drop the angle parameter from $\mathbf{a}_R(\theta_R)$ and $\mathbf{a}_T(\theta_T)$. These two vectors are normalized so that $\|\mathbf{a}_R\|^2 = \|\mathbf{a}_T\|^2 = 1$. Therefore, the received signal at the analog output of the array at a time instant t, can be written as

$$\begin{aligned}\mathbf{r}(t) &\triangleq [r_1(t), r_2(t), ..., r_{N_R}(t)]^T, \quad \in \mathbb{C}^{N_R}, t \in [0, T_o], \\ &= \mathbf{H}\mathbf{x}(t-\tau) + \mathbf{n}(t). \end{aligned} \tag{1}$$

where $T_o = N_s T_s$ is the observation time and N_s is the number of pilot symbols. Moreover, $\tau \in \mathbb{R}^+$ is the propagation delay of the transmitted signal and is related to the transmitter-receiver distance , D_0, by $\tau = D_0/c$. Furthermore, $\mathbf{n}(t) \triangleq [n_1(t), n_2(t), ..., n_{N_T}(t)]^T \in \mathbb{C}^{N_R}$ denotes zero-mean additive white Gaussian noise processes with noise power $\sigma_n^2 \triangleq WN_0/2$, where $N_0/2$ is the noise spectral density, and W is the signal bandwidth. Furthermore, $\mathbf{x}(t) \triangleq [x_1(t), x_2(t), ..., x_{N_T}(t)]^T \in \mathbb{C}^{N_T}$ is the transmitted signal vector at the output of a beamforming matrix $\mathbf{F} \triangleq [\mathbf{f}_1, \mathbf{f}_2, ...\mathbf{f}_{N_B}]$ such that $\mathbf{x}(t) = \sqrt{P_t}\mathbf{F}\mathbf{s}(t)$ and $\mathbf{s}(t) \triangleq [s_1(t), s_2(t), ..., s_{N_B}(t)]^T$, where N_B is the number of transmitted beams and P_t is the transmitted power. Moreover,

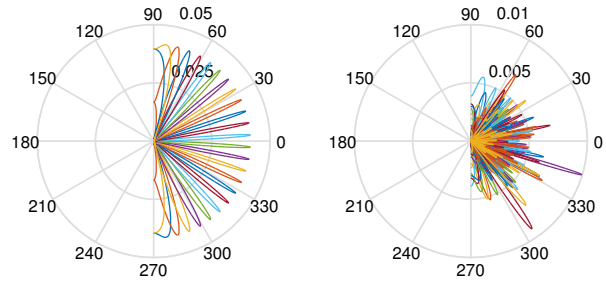

Fig. 2. Beam patterns generated using DBF (left) and RPBF (right) with N_T=32 and N_B=24. For directional beamforming, $\psi_\ell = (-90° + 7.2°\ell)$.

$$s_\ell(t) = \sum_{k=0}^{N_s-1} a_{\ell,k} p(t - kT_s), \ell = 1, ..., N_B$$

where $a_{\ell,k}$ is the kth pilot symbol transmitted over the ℓth beam, and $p(t)$ is a unit-energy pulse. To keep the transmitted power fixed, regardless of the number of antennas, N_T, we normalize $\mathbf{F}$ such that $\mathrm{Tr}\left(\mathbf{F}^H\mathbf{F}\right) = 1$, and $\mathbb{E}\{\mathbf{s}(t)\mathbf{s}^H(t)\} = \mathbf{I}$. Matrix $\mathbf{F}$ is modeled in two ways: directional and random. These models and the differences between them are discussed in detail in the sequel of Section III.

Our aim is to investigate the impact of beamforming schemes on the estimation lower bounds of $\boldsymbol{\phi} = [\theta_R, \theta_T, \beta, \tau]^T$ based on the observed signal, $\mathbf{r}(t)$.

III. Random-Phase Beamforming and Directional Beamforming

In this section, the two considered beamforming schemes are defined. The impact of these two schemes on the joint estimation of DOD, DOA, TOA and channel gain is investigated in subsequent sections. The first scheme we consider is DBF, which spatially steers the transmission beams towards the azimuth angles $\psi_\ell, 1 \le \ell \le N_B$ such that

$$\mathbf{f}_\ell \triangleq \frac{1}{\sqrt{N_B}}\mathbf{a}_T(\psi_\ell), \tag{2}$$

where d, and λ denote the inter-antenna spacing and the carrier wavelength, respectively. The DBF in (2) has been used in several works on mm-wave, for example, see [11].

On the other hand, the RPBF generate beams with uniformly distributed random phases such that

$$\mathbf{f}_\ell \triangleq \frac{1}{\sqrt{N_T N_B}}[e^{j\vartheta_{\ell,1}}, ..., e^{j\vartheta_{\ell,N_T}}]^T, \tag{3}$$

where $\vartheta_{\ell,n} \sim U(0, 2\pi)$. Although, practical phase shifters generate quantized phases, recently, phase shifters for mm-wave with 3.5° phase resolution were proposed [15], [16].

Note that in (3) the phase is random, in contrast to the scheme in [8], [9], which have a structure similar to (2), but with a random direction. Moreover, note that both (2) and (3) have $\|\mathbf{f}_\ell\|^2 = \frac{1}{N_B}$. This implies that increasing the number of beams,

will linearly scale down the power per beam to preserve the constant transmitted power condition.

A nice feature of (3) is that the generated beams are not too narrow compared to those of DBF as shown in Fig. 2. Thus, RPBF exhibits a better spatial coverage, which is an essential feature when the initial direction of transmission is unknown.

IV. Cramér-Rao Lower Bound

A widely used performance measures in estimation theory is the Cramér-Rao lower bound (CRB) [17]. CRB provides a lower bound for the variance of an unbiased estimator of a given parameter. We use the CRB to compare the best performance of RPBF and DBF in the scenario described in Section II.

The CRB of estimating $\boldsymbol{\phi}$ for an arbitrary array geometry is derived in Appendix A. Subsequently, for the case of ULA, we show in Appendix B that the CRBs for jointly estimating $\theta_R, \theta_T, \beta$ and τ are given by

$$\mathrm{CRB}(\theta_R) = \frac{12}{\gamma N_R^3 [\mathbf{Q}]_{1,1}} \Big(\frac{\lambda}{2\pi d \cos\theta_R}\Big)^2, \tag{4}$$

$$\mathrm{CRB}(\theta_T) = \frac{[\mathbf{Q}]_{1,1}}{\gamma N_R \ \det(\mathbf{Q})} \Big(\frac{\lambda}{2\pi d \cos\theta_T}\Big)^2, \tag{5}$$

$$\mathrm{CRB}(\beta) = \frac{2|\beta|^2}{\gamma N_R [\mathbf{Q}]_{1,1}} \left(\frac{2N_R - 1}{N_R + 1} + \frac{[\mathbf{Q}]_{1,1}[\mathbf{Q}]_{2,2}}{2\det(\mathbf{Q})}\right), \tag{6}$$

$$\mathrm{CRB}(\tau) = \frac{1}{\gamma \sigma_p^2 N_R [\mathbf{Q}]_{1,1}}. \tag{7}$$

where $\gamma = N_T N_s P_t |\beta|^2/\sigma_n^2$ and $\sigma_p^2 \triangleq \int_{-\infty}^{\infty} \left(\frac{\partial p(t)}{\partial \tau}\right)^2 dt$,

$$\mathbf{Q} \triangleq \begin{bmatrix} \mathbf{a}_T^H \mathbf{F}\mathbf{F}^H \mathbf{a}_T & \mathbf{a}_T^H \mathbf{D}_T \mathbf{F}\mathbf{F}^H \mathbf{a}_T \\ \mathbf{a}_T^H \mathbf{D}_T \mathbf{F}\mathbf{F}^H \mathbf{a}_T & \mathbf{a}_T^H \mathbf{D}_T \mathbf{F}\mathbf{F}^H \mathbf{D}_T \mathbf{a}_T \end{bmatrix},$$

and $\mathbf{D}_T \triangleq \mathrm{diag}(0, 1, 2, ..., N_T - 1)$.

A. DBF Analysis

Define $\varphi_\ell \triangleq (2\pi d/\lambda)\big(\sin\theta_T - \sin\psi_\ell\big)$. Then, for DBF

$$[\mathbf{Q}]_{1,1} = \frac{1}{N_T^2 N_B} \sum_{\ell=1}^{N_b} \frac{1 - \cos N_T \varphi_\ell}{1 - \cos\varphi_\ell}, \tag{8}$$

$$[\mathbf{Q}]_{2,2} = \frac{1}{2N_T^2 N_B} \sum_{\ell=1}^{N_b} \frac{N_T^2 - N_T}{1 - \cos\varphi_\ell} + \frac{1 + \cos N_T \varphi}{(1 - \cos\varphi_\ell)^2}, \tag{9}$$

$$Q_r \triangleq \Re\{[\mathbf{Q}]_{1,2}\} = \frac{(N_T - 1)}{2} [\mathbf{Q}]_{1,1}, \tag{10}$$

$$Q_i \triangleq \Im\{[\mathbf{Q}]_{1,2}\} = \frac{1}{N_T^2 N_B} \times \tag{11}$$

$$\sum_{\ell=1}^{N_b} \frac{(1 - \cos N_T \varphi_\ell)\sin\varphi_\ell - N_T\,(1 - \cos\varphi_\ell)\sin N_T \varphi_\ell}{(1 - \cos\varphi_\ell)^2}.$$

Note that (8)–(11) imply that the performance of DBF is highly governed by the difference between θ_T and ψ_ℓ. Ideally, the difference should be zero to achieve the lowest CRB. Moreover, carefully inspecting (8)–(11), one can notice the averaging over N_B. Thus, after a certain value of N_B, increasing N_B has a little effect on the CRBs, and a performance floor is reached.

Since N_T and N_B will be typically very large, it is meaningful to analyze the limiting behavior of the elements and determinant of $\mathbf{Q}$ with N_T. When considering the relationship between DBF CRB and N_T, we can see that there are two components in (8)–(11); a short-term harmonic component represented by $\cos(N_T\varphi)$ and a long-time trend represented by a polynomial of N_T. Focusing on the long-term trend, it can be noticed that $[\mathbf{Q}]_{1,1} \sim \mathcal{O}(\frac{1}{N_T^2})$, the real and imaginary parts of $[\mathbf{Q}]_{1,2} \sim \mathcal{O}(\frac{1}{N_T}), \det(\mathbf{Q}) \sim \mathcal{O}(\frac{1}{N_T^2})$, while $[\mathbf{Q}]_{2,2}$ is constant. Consequently, we can deduce that $\mathrm{CRB}(\theta_R) \sim \mathcal{O}(N_T), \mathrm{CRB}(\theta_T) \sim \mathcal{O}(\frac{1}{N_T}), \mathrm{CRB}(\beta) \sim \mathcal{O}(N_T)$, and $\mathrm{CRB}(\tau) \sim \mathcal{O}(N_T)$.

Due to the fixed transmit power constraint, higher N_T means narrower beams, and higher received power in a certain direction as implied by (2). If that direction mismatches θ_T, the CRBs of $\theta_R, \beta,$ and τ tend to worsen when N_T increases.

B. RPBF Analysis

For the RPBF case, since both N_T and N_B are typically high, we resort to the law of large numbers to compute the average CRB. Denoting the expected value by $\mathbb{E}\{\cdot\}$, we calculate $\mathbb{E}\{[\mathbf{Q}]_{1,1}\}$, $\mathbb{E}\{[\mathbf{Q}]_{2,2}\}$, and $\mathbb{E}\{\det(\mathbf{Q})\}$, to obtain the limiting behavior of (4)–(7) as

$$\mathbb{E}\{[\mathbf{Q}]_{1,1}\} = \mathbf{a}_T^H \mathbb{E}\{\mathbf{F}\mathbf{F}^H\}\mathbf{a}_T = \frac{\mathbf{a}_T^H \mathbf{a}_T}{N_T} = \frac{1}{N_T}, \tag{12}$$

$$\mathbb{E}\{[\mathbf{Q}]_{2,2}\} = \frac{\mathbf{a}_T^H \mathbf{D}_T^2 \mathbf{a}_T}{N_T} = \frac{\sum_{i=0}^{N_T-1} i^2}{N_T^2} \approx \frac{N_T}{3}, \tag{13}$$

$$\mathbb{E}\{[\mathbf{Q}]_{1,2}\} = \frac{\mathbf{a}_T^H \mathbf{D}_T \mathbf{a}_T}{N_T} = \frac{\sum_{i=0}^{N_T-1} i}{N_T^2} \approx \frac{1}{2}, \tag{14}$$

$$\mathbb{E}\{\det(\mathbf{Q})\} \approx \frac{1}{N_T}\frac{N_T}{3} - \Big(\frac{1}{2}\Big)^2 = \frac{1}{12}. \tag{15}$$

The results in (12)–(15) imply that $\mathrm{CRB}(\theta_T) \sim \mathcal{O}(1/N_T^2)$, while $\mathrm{CRB}(\theta_R), \mathrm{CRB}(\beta),$ and $\mathrm{CRB}(\tau)$ are constant in N_T and N_B. In contrast to DBF, increased N_T does not decrease the spatial coverage. Thus, higher N_T does not affect the received power in average, and the CRBs of $\theta_R, \beta,$ and τ stay constant.

V. Simulation and Numerical Results

With reference to the scenario illustrated in Fig. 1, we consider a receiver equipped with a ULA lying in the x-axis with $d = \lambda/2$, and covering a spatial field $(-\pi/2, \pi/2)$. The transmitter, operating at $f = 38$ GHz, is assumed to be tilted with an orientation angle α measured from the positive x-axis. Without loss of generality, we select $\alpha = 0$. The DODs and DOAs are measured clockwise from the line normal to the array. The BS is assumed to be located at the origin, while the UE is located at $\mathbf{p} = (5, 25)$ meter. This results in $\theta_R = \theta_T = 11.3°$. Similar to [18], the complex channel gain is computed using the free-space propagation model, leading to $\beta = \beta_R + j\beta_I = -(56.5 + j53.7) \times 10^{-3}$. Moreover, we consider $p(t)$ to be a unit-energy ideal $sinc$ pulse. Consequently, it follows from Parseval's theorem that

$$\sigma_p^2 = \frac{4}{3}\pi^2 W^2, \tag{16}$$

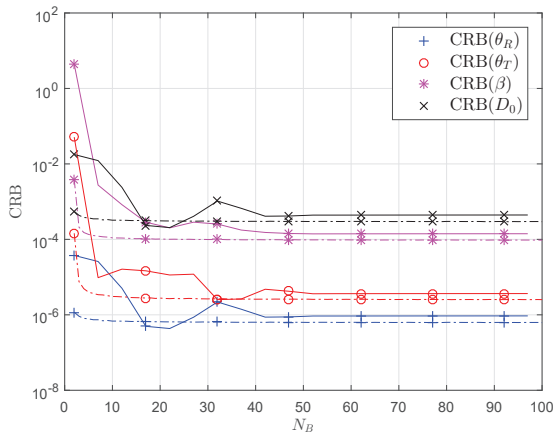

Fig. 3. CRB w.r.t N_B using RPBF (dashed line) and DBF (solid line) with $N_R = 64, N_T = 32$. Directional beams are equally spaced over (-$\pi/2, \pi/2$)

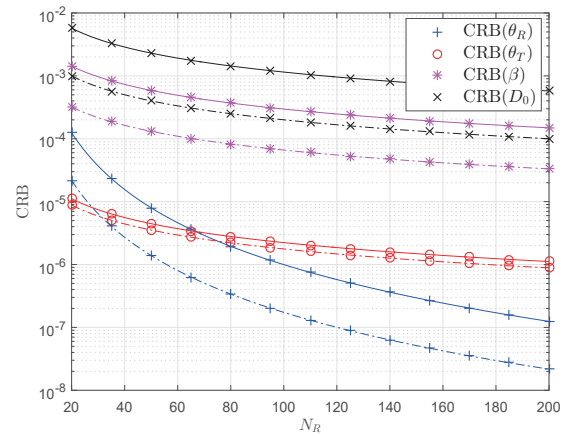

Fig. 4. CRB w.r.t N_R using RPBF (dashed line) and DBF (solid line) with $N_B = 18, N_T = 32$. Directional beams are equally spaced over (-$\pi/2, \pi/2$)

where $W = R_b/2b$, and R_b is the bit rate, and b is the number of bits per symbol. We present the results for 1 Gbps bit rate and 16 QAM transmission, i.e., W = 125 MHz. Furthermore, we assume $\sigma_n^2 = 20$ dBm, and $P_t = 1$ W. To improve the results presentation, we provide the $\mathrm{CRB}(\tau)$ in terms of $\mathrm{CRB}(D_0)$.

For DBF, the directions are chosen to be equally spaced to cover the region $(-\pi/2, \pi/2)$, i.e., $\psi_\ell = -\frac{\pi}{2} + \frac{\pi\ell}{N_B+1}, 1 \leq \ell \leq N_B$. Finally, in the following results, when referring to RPBF, CRB means the average CRB. RPBF plots are obtained by Monte-Carlo simulation averaged over 1000 iteration.

A. Effect of N_B on the CRB

Fig. 3 illustrates the CRB as a function of N_B with $N_T = 32$ and $N_R = 64$. It can be seen that, using RPBF, the CRB floor is reached at $N_B = 18$. Also, note that for $N_B < 10$ the average CRBS of θ_R and D_0 are less sensitive to N_B compared to those of θ_T, and β. On the other hand, the CRB under DBF is non-monotonic. Thus, N_B should be carefully chosen for optimum estimation. However, since in the initial access phase the transmitter has no information on the direction of transmission, an optimal beam is not guaranteed.

Comparing RPBF with DBF in Fig. 3, it can be inferred that the RPBF scheme attains a lower floor at a low N_B than the DBF, except when the latter happens to have a beam close to the receiver direction. To see why the CRB floors, notice the averaging effect in (8)–(11), and the independence of N_B in (12)–(15). Intuitively, recall that with a fixed N_R the receiver beam-width about θ_R is fixed. Consider the RPBF case shown in Fig. 2. When N_B is small, there is a limited chance that a random transmit beam will hit θ_R with a suitable gain, but as N_B goes up, this chance enhances and the CRB starts to decrease. As N_B grows significantly, the resultant beams becomes almost omni-directional and, regardless of how high N_B is, the CRB becomes fixed. On the other hand, consider the DBF case in Fig. 2, where beams have a comb-like shape and the CRB mainly depends on the difference between the transmit beams and the receive beam. As N_B grows higher, more transmit beams fall within the the receive beam-width. However, since $\|\mathbf{f}_\ell\|^2 = 1/N_B$, the received power stays fixed, and the CRB floor is reached.

B. Effect of N_R on the CRB

The CRBs as function of N_R are provided in Fig. 4. In both schemes, CRBs of θ_T, β, and τ decrease as $1/N_R$. On the other hand, CRB of θ_R decreases by three orders of magnitude, when N_R increases by one order of magnitude. In addition, these results confirm the conclusion made using Fig. 3 in that RPBF provides better bounds than DBF does, when N_B is fixed.

C. Effect of N_T on the CRB

Fig. 5 illustrates the results of investigating the CRB in terms of N_T. Considering DBF, it is hard to draw any conclusion for scaling factors in terms of N_T due to the high non-linearity observed and represented by (8)–(11). However, there is an average trend that can be seen, as discussed in Section IV, whereby $\mathrm{CRB}(\theta_T)$ decreases with $1/N_T^2$ while the other CRBs increase with N_T. As for RPBF, it can be seen from the figure that only the estimation of θ_T improves when increasing N_T. Note that due to the power normalization discussed in Section II, the CRBs of β and θ_R are not affected by an increased N_T.

D. Summary of Results

From Figs. 3 – 5, it can be inferred that RPBF outperforms DBF in terms of the channel parameters CRBs, except in some cases shown in Fig. 3, where a few N_B choices can results in a better DBF performance. Note that in these cases a beam or more are close enough to the receiver direction, hence the better CRB. However, since at the IA stage the receiver location is unknown, a careful choice of N_B cannot be made for DBF. As a result, RBPF is more reliable in this case during AI phase.

VI. Conclusion

Mm-wave MIMO is a very promising technology for future mobile communication. In this paper, we have studied the impact of two beamforming schemes on the CRB of estimating DOA, DOD, TOA, and complex channel gain. RPBF has shown better CRB floor at a smaller number of beams than DBF. Thus, as shown by the numerical results, it would be favorable to use RPBF in the initial access phase. Table I summarizes the CRB scaling factors in terms of N_R, N_T and N_B. As future work, we will consider mm-wave channels with multi-path propagation and carry out an analytical investigation of RPBF and DBF.

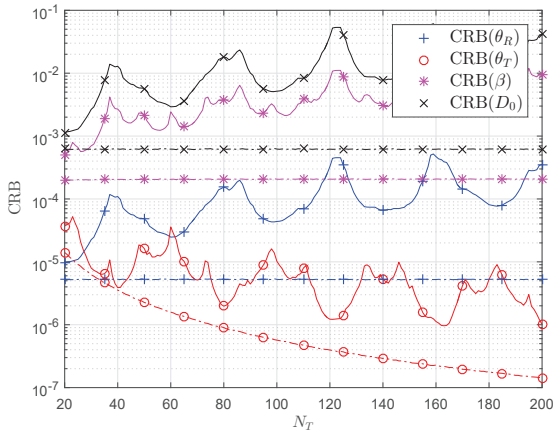

Fig. 5. CRB w.r.t N_T using RPBF (dashed line) and DBF (solid line) with $N_B = 18, N_R = 32$. Directional beams are equally spaced over (-$\pi/2, \pi/2$)

Appendix A
CRB(ϕ) for An arbitrary Geometry

Consider the received signal model in (1). Let

$$\boldsymbol{\mu}(\boldsymbol{\phi}) \triangleq \mathbf{H}\mathbf{x}(t-\tau) = \sqrt{N_R N_T P_t}\beta \mathbf{a}_R \mathbf{a}_T^H \mathbf{F}\mathbf{s}(t-\tau).$$

Using arbitrary array geometries at the transmitter and receiver, the corresponding steering vectors are given by

$$\mathbf{a}_T = \frac{1}{\sqrt{N_T}} e^{-j\mathbf{k}^T(\theta_T)\mathbf{v}_{n_t}}, n_t = 1, 2, ..., N_T. \tag{17}$$

$$\mathbf{a}_R = \frac{1}{\sqrt{N_R}} e^{-j\mathbf{k}^T(\theta_R)\mathbf{u}_{n_r}}, n_r = 1, 2, ..., N_R, \tag{18}$$

where $\mathbf{k}^T(\theta) = \frac{2\pi}{\lambda}[\sin(\theta), \cos(\theta)]$ is the wavenumber vector, and $\mathbf{u}_n$ and $\mathbf{v}_n$ are vectors of the Cartesian coordinates of the nth antenna at the receiver and the transmitter, in meters, respectively. We start by computing FIM

$$[\mathbf{I}(\boldsymbol{\phi})]_{p,q} \triangleq \frac{1}{\sigma_n^2} \int_0^{T_o} \Re\left\{ \left(\frac{\partial \boldsymbol{\mu}^H(\boldsymbol{\phi})}{\partial \phi_p}\right)\left(\frac{\partial \boldsymbol{\mu}(\boldsymbol{\phi})}{\partial \phi_q}\right)\right\} dt, \tag{19}$$

where ϕ_p is the pth element in $\boldsymbol{\phi}$, $1 \le p, q \le 5$. Consequently,

$$\frac{\partial \boldsymbol{\mu}(\boldsymbol{\phi})}{\partial \theta_R} = -j\sqrt{N_R N_T P_t}\beta_m \mathbf{K}_R \mathbf{a}_R \mathbf{a}_T^H \mathbf{F}\mathbf{s}(t-\tau), \tag{20}$$

$$\frac{\partial \boldsymbol{\mu}(\boldsymbol{\phi})}{\partial \theta_T} = j\sqrt{N_R N_T P_t}\beta_m \mathbf{a}_R \mathbf{a}_T^H \mathbf{K}_T \mathbf{F}\mathbf{s}(t-\tau), \tag{21}$$

$$\frac{\partial \boldsymbol{\mu}(\boldsymbol{\phi})}{\partial \beta_R} = \sqrt{N_R N_T P_t}\mathbf{a}_R \mathbf{a}_T^H \mathbf{F}\mathbf{s}(t-\tau), \tag{22}$$

$$\frac{\partial \boldsymbol{\mu}(\boldsymbol{\phi})}{\partial \beta_I} = j\sqrt{N_R N_T P_t}\mathbf{a}_R \mathbf{a}_T^H \mathbf{F}\mathbf{s}(t-\tau), \tag{23}$$

$$\frac{\partial \boldsymbol{\mu}(\boldsymbol{\phi})}{\partial \tau} = -\sqrt{P_t}\mathbf{H}\mathbf{F}\frac{\partial \mathbf{s}(t-\tau)}{\partial \tau}, \tag{24}$$

$$\mathbf{K}_R \triangleq \text{diag}\left(\frac{\partial \mathbf{k}^T(\theta_R)}{\partial \theta_R}[\mathbf{u}_1, \mathbf{u}_2, ..., \mathbf{u}_{N_R}]\right),$$

$$\mathbf{K}_T \triangleq \text{diag}\left(\frac{\partial \mathbf{k}^T(\theta_T)}{\partial \theta_T}[\mathbf{v}_1, \mathbf{v}_2, ..., \mathbf{v}_{N_T}]\right).$$

Define the following matrices

$$\boldsymbol{\Sigma}_0 \triangleq \int_0^{T_o} \mathbf{s}(t-\tau)\mathbf{s}^H(t-\tau)\, dt = N_s \mathbf{I},$$

TABLE I
Scaling Effect on CRBs For High N_T And N_B.

	N_R	N_T (RPBF)	N_T (DBF)	N_B
CRB(θ_R)	$\frac{1}{N_R^3}$	constant	$\mathcal{O}(N_T)$	constant
CRB(θ_T)	$\frac{1}{N_R}$	$\mathcal{O}\left(\frac{1}{N_T^2}\right)$	$\mathcal{O}\left(\frac{1}{N_T}\right)$	constant
CRB(β)	$\frac{1}{N_R}$	constant	$\mathcal{O}(N_T)$	constant
CRB(τ)	$\frac{1}{N_R}$	constant	$\mathcal{O}(N_T)$	constant

$$\boldsymbol{\Sigma}_1 \triangleq \int_0^{T_o} \mathbf{s}(t-\tau)\frac{\partial \mathbf{s}^H(t-\tau)}{\partial \tau} dt = \mathbf{0},$$

$$\boldsymbol{\Sigma}_2 \triangleq \int_0^{T_o} \frac{\partial \mathbf{s}(t-\tau)}{\partial \tau}\frac{\partial \mathbf{s}^H(t-\tau)}{\partial \tau} dt$$

$$= \int_{-\infty}^{\infty} \left(\frac{\partial p(t-\tau)}{\partial \tau}\right)^2 dt N_s \mathbf{I} \triangleq \sigma_p^2 N_s \mathbf{I}.$$

Note that the derivative of an even function is odd, and the product of an even and an odd functions is odd. The integral of an odd function over its domain is zero. Consequently, $\boldsymbol{\Sigma}_1 = \mathbf{0}$.

From Section II, $\phi_1 = \theta_R$. Thus, substituting (20) into (19), and using $\mathbf{a}^H\mathbf{b}\mathbf{c}^H\mathbf{d} = \mathbf{c}^H\mathbf{d}\mathbf{a}^H\mathbf{b}$, it is easy to show that

$$[\mathbf{I}(\boldsymbol{\phi})]_{1,1} = \frac{N_R N_T N_s P_t |\beta|^2}{\sigma_n^2}\mathbf{a}_R^H \mathbf{K}_R^2 \mathbf{a}_R \mathbf{a}_T^H \mathbf{F}\mathbf{F}^H \mathbf{a}_T. \tag{25}$$

Define $\zeta \triangleq N_T N_s P_t/\sigma_n^2$. Subsequently, it can be shown that

$$[\mathbf{I}(\boldsymbol{\phi})]_{2,2} = \zeta N_R |\beta|^2 \mathbf{a}_T^H \mathbf{K}_T \mathbf{F}\mathbf{F}^H \mathbf{K}_T \mathbf{a}_T, \tag{26}$$

$$[\mathbf{I}(\boldsymbol{\phi})]_{3,3} = [\mathbf{I}(\boldsymbol{\phi})]_{4,4} = \zeta N_R \mathbf{a}_T^H \mathbf{F}\mathbf{F}^H \mathbf{a}_T, \tag{27}$$

$$[\mathbf{I}(\boldsymbol{\phi})]_{5,5} = \frac{P_t N_s \sigma_p^2}{\sigma_n^2}\text{Tr}(\mathbf{H}\mathbf{F}\mathbf{F}^H\mathbf{H}^H), \tag{28}$$

$$[\mathbf{I}(\boldsymbol{\phi})]_{1,2} = -\zeta N_R |\beta|^2 \mathbf{a}_R^H \mathbf{K}_R \mathbf{a}_R \Re\{\mathbf{a}_T^H \mathbf{K_T F}\ \mathbf{F}^H \mathbf{a}_T\}, \tag{29}$$

$$[\mathbf{I}(\boldsymbol{\phi})]_{1,3} = \zeta N_R \beta_I \mathbf{a}_R^H \mathbf{K}_R \mathbf{a}_R \mathbf{a}_T^H \mathbf{F}\mathbf{F}^H \mathbf{a}_T, \tag{30}$$

$$[\mathbf{I}(\boldsymbol{\phi})]_{1,4} = -\zeta N_R \beta_R \mathbf{a}_R^H \mathbf{K}_R \mathbf{a}_R \mathbf{a}_T^H \mathbf{F}\mathbf{F}^H \mathbf{a}_T, \tag{31}$$

$$[\mathbf{I}(\boldsymbol{\phi})]_{2,3} = -\zeta N_R \Re\{j\beta^* \mathbf{a}_T^H \mathbf{F}\mathbf{F}^H \mathbf{K}_T \mathbf{a}_T\}, \tag{32}$$

$$[\mathbf{I}(\boldsymbol{\phi})]_{2,4} = \zeta N_R \Re\{\beta^* \mathbf{a}_T^H \mathbf{F}\mathbf{F}^H \mathbf{K}_T \mathbf{a}_T\}, \tag{33}$$

$$[\mathbf{I}(\boldsymbol{\phi})]_{1,5} = [\mathbf{I}(\boldsymbol{\phi})]_{2,5} = [\mathbf{I}(\boldsymbol{\phi})]_{3,5} \tag{34}$$

$$= [\mathbf{I}(\boldsymbol{\phi})]_{4,5} = [\mathbf{I}(\boldsymbol{\phi})]_{3,4} = 0. \tag{35}$$

Now that we obtained FIM, the CRB can be derived from [17]

$$\text{CRB}(\boldsymbol{\phi}) = \text{diag}\left(\mathbf{I}^{-1}(\boldsymbol{\phi})\right). \tag{36}$$

From (25)–(35), it can be seen that $\mathbf{I}(\boldsymbol{\phi})$ is block diagonal. Thus, for $\bar{\boldsymbol{\phi}} = [\theta_R, \theta_T, \beta_R, \beta_I]^T$, (36) can be written as

$$\text{CRB}(\boldsymbol{\phi}) = \begin{bmatrix} \text{diag}\left(\mathbf{I}^{-1}(\bar{\boldsymbol{\phi}})\right) \\ [\mathbf{I}(\boldsymbol{\phi})]_{5,5}^{-1} \end{bmatrix}. \tag{37}$$

To compute $\mathbf{I}^{-1}(\bar{\boldsymbol{\phi}})$, we start by defining the following

$$\begin{bmatrix} R_1 \\ R_2 \end{bmatrix} \triangleq \begin{bmatrix} \mathbf{a}_R^H \mathbf{K}_R \mathbf{a}_R \\ \mathbf{a}_R^H \mathbf{K}_R^2 \mathbf{a}_R \end{bmatrix}, \begin{bmatrix} T_1 \\ T_2 \\ T_3 \end{bmatrix} \triangleq \begin{bmatrix} \mathbf{a}_T^H \mathbf{F}\mathbf{F}^H \mathbf{a}_T \\ \mathbf{a}_T^H \mathbf{K}_T \mathbf{F}\mathbf{F}^H \mathbf{a}_T \\ \mathbf{a}_T^H \mathbf{K}_T \mathbf{F}\mathbf{F}^H \mathbf{K}_T \mathbf{a}_T \end{bmatrix},$$

$$\begin{bmatrix} S_1 \\ S_2 \end{bmatrix} \triangleq \begin{bmatrix} -(\beta_I T_R + \beta_R T_I) \\ \beta_R Tr - \beta_I T_I \end{bmatrix}, T_2 \triangleq T_R + jT_I,$$

and $\gamma \triangleq N_T N_s P_t |\beta|^2/\sigma_n^2$. Consequently, from (25)–(35),

$$\mathbf{I}(\bar{\phi}) \triangleq \frac{\gamma N_r}{|\beta|^2} \begin{bmatrix} \mathbf{A} & \mathbf{U} \\ \mathbf{U}^T & \mathbf{C} \end{bmatrix} = \frac{\gamma N_r}{|\beta|^2} \times \tag{38}$$

$$\left[\begin{array}{cc:cc} |\beta|^2 R_2 T_1 & -|\beta|^2 R_1 T_R & \beta_I R_1 T_1 & -\beta_R R_1 T_1 \\ -|\beta|^2 R_1 T_R & |\beta|^2 T_3 & S_1 & S_2 \\ \hdashline \beta_I R_1 T_1 & S_1 & T_1 & 0 \\ -\beta_R R_1 T_1 & S_2 & 0 & T_1 \end{array}\right]$$

By block-matrix inversion,

$$\mathrm{CRB}\left(\begin{bmatrix} \theta_R \\ \theta_T \end{bmatrix}\right) = \frac{|\beta|^2}{\gamma N_R} \operatorname{diag}\left[\left(\mathbf{A} - \mathbf{U}\mathbf{C}^{-1}\mathbf{U}^T\right)^{-1}\right], \tag{39}$$

$$\mathrm{CRB}\left(\begin{bmatrix} \beta_R \\ \beta_I \end{bmatrix}\right) = \frac{|\beta|^2}{\gamma N_R} \operatorname{diag}\Big[\mathbf{C}^{-1}\mathbf{U}^T \left(\mathbf{A} - \mathbf{U}\mathbf{C}^{-1}\mathbf{U}^T\right)^{-1} \mathbf{U}\mathbf{C}^{-1} + \mathbf{C}^{-1}\Big] \tag{40}$$

We now proceed to evaluate (39) and (40). Directly from (38),

$$\mathbf{A} - \mathbf{U}\mathbf{C}^{-1}\mathbf{U}^T = |\beta|^2 \begin{bmatrix} T_1(R_2 - R_1^2) & 0 \\ 0 & \frac{(T_1 T_3 - |T_2|^2)}{T_1} \end{bmatrix}, \tag{41}$$

$$\mathbf{C}^{-1}\mathbf{U}^T \left(\mathbf{A} - \mathbf{U}\mathbf{C}^{-1}\mathbf{U}^T\right)^{-1} \mathbf{U}\mathbf{C}^{-1} + \mathbf{C}^{-1} = \frac{1}{|\beta|^2 T_1} \times$$

$$\begin{bmatrix} \frac{\beta_I^2 R_1^2}{R_2 - R_1^2} + \frac{S_1}{T_1 T_3 - |T_2|^2} + |\beta|^2 \frac{-\beta_I \beta_R R_1^2}{R_2 - R_1^2} + \frac{S_1 S_2}{T_1 T_3 - |T_2|^2} \\ \frac{-\beta_I \beta_R R_1^2}{R_2 - R_1^2} + \frac{S_1 S_2}{T_1 T_3 - |T_2|^2} \; \frac{\beta_R^2 R_1^2}{R_2 - R_1^2} + \frac{S_2}{T_1 T_3 - |T_2|^2} + |\beta|^2 \end{bmatrix}. \tag{42}$$

Appendix B
CRB for a ULA

For a ULA,

$$\begin{aligned} R_1 &= (2\pi d/\lambda)\cos(\theta_R)\mathbf{a}_R^H \mathbf{D}_R \mathbf{a}_R \\ &= (\pi d/\lambda)\cos(\theta_R)\left(N_R - 1\right), \end{aligned} \tag{43}$$

$$\begin{aligned} R_2 &= (2\pi d/\lambda)^2 \cos^2(\theta_R)\mathbf{a}_R^H \mathbf{D}_R^2 \mathbf{a}_R \\ &= \frac{2}{3}(\pi d/\lambda)^2 \cos^2(\theta_R)(N_R - 1)(2N_R - 1), \end{aligned} \tag{44}$$

where $\mathbf{D}_R = \operatorname{diag}(0, 1, 2, ..., N_R - 1)$. Moreover

$$\begin{bmatrix} T_1 & T_2 \\ T_2 & T_3 \end{bmatrix} = \begin{bmatrix} [\mathbf{Q}]_{1,1} & \frac{2\pi d}{\lambda}\cos(\theta_R)[\mathbf{Q}]_{1,2} \\ \frac{2\pi d}{\lambda}\cos(\theta_R)[\mathbf{Q}]_{1,2} & \left(\frac{2\pi d}{\lambda}\right)^2 \cos^2(\theta_R)[\mathbf{Q}]_{2,2} \end{bmatrix} \tag{45}$$

where $\mathbf{Q} \triangleq \begin{bmatrix} \mathbf{a}_T^H \mathbf{F}\mathbf{F}^H \mathbf{a}_T & \mathbf{a}_T^H \mathbf{D}_T \mathbf{F}\mathbf{F}^H \mathbf{a}_T \\ \mathbf{a}_T^H \mathbf{D}_T \mathbf{F}\mathbf{F}^H \mathbf{a}_T & \mathbf{a}_T^H \mathbf{D}_T \mathbf{F}\mathbf{F}^H \mathbf{D}_T \mathbf{a}_T \end{bmatrix}$, $\mathbf{D}_T \triangleq \operatorname{diag}(0, 1, 2, ..., N_T - 1)$, and $[\mathbf{Q}]_{1,2} \triangleq Q_R + jQ_I$.

Substituting (43)–(45) in (41), then in (39) yields

$$\mathrm{CRB}(\theta_R) = \frac{12}{\gamma N_R^3 [\mathbf{Q}]_{1,1}} \left(\frac{\lambda}{2\pi d \cos\theta_R}\right)^2,$$

$$\mathrm{CRB}(\theta_T) = \frac{[\mathbf{Q}]_{1,1}}{\gamma N_R \ \det(\mathbf{Q})} \left(\frac{\lambda}{2\pi d \cos\theta_T}\right)^2.$$

Note that since β_R and β_I are independent, the CRB of β can be simplified to $\mathrm{CRB}(\beta) = \mathrm{CRB}(\beta_R) + \mathrm{CRB}(\beta_I)$. Thus, substituting (43)–(45) in (42), and taking the trace, yields

$$\mathrm{CRB}(\beta) = \frac{2|\beta|^2}{\gamma N_R [\mathbf{Q}]_{1,1}} \left[\frac{2N_R - 1}{N_R + 1} + \frac{[\mathbf{Q}]_{1,1}[\mathbf{Q}]_{2,2}}{2\det(\mathbf{Q})}\right].$$

Finally, following from (28) and (37), it is easy to see that

$$\mathrm{CRB}(\tau) = \frac{1}{\gamma \sigma_p^2 N_R [\mathbf{Q}]_{1,1}}.$$

Acknowledgment

This work is partly supported by the Horizon2020 project HIGHTS (High precision positioning for cooperative ITS applications) MG-3.5a-2014-636537, the Australian Research Council's Discovery Projects funding scheme under Project DP140101133, and the Spanish Grant TEC2014-53656-R.

References

[1] J. G. Andrews, S. Buzzi, W. Choi, S. V. Hanly, A. Lozano, A. C. K. Soong, and J. C. Zhang, "What will 5G be?" *IEEE J. Sel. Areas Commun.*, vol. 32, no. 6, pp. 1065–1082, June 2014.

[2] T. S. Rappaport, S. Sun, R. Mayzus, H. Zhao, Y. Azar, K. Wang, G. N. Wong, J. K. Schulz, M. Samimi, and F. Gutierrez, "Millimeter wave mobile communications for 5G cellular: It will work!" *IEEE Access*, vol. 1, pp. 335–349, 2013.

[3] Z. Pi and F. Khan, "An introduction to millimeter-wave mobile broadband systems," *IEEE Commun. Mag.*, vol. 49, no. 6, pp. 101–107, June 2011.

[4] R. Heath, N. Gonzalez-Prelcic, S. Rangan, W. Roh, and A. Sayeed, "An overview of signal processing techniques for millimeter wave MIMO systems," *IEEE J. Sel. Topics Signal Process.*, no. 99, 2016.

[5] S. Sun, G. R. MacCartney, M. K. Samimi, and T. S. Rappaport, "Synthesizing omnidirectional antenna patterns, received power and path loss from directional antennas for 5G millimeter-wave communications," in *2015 IEEE Global Commun. Conf. (GLOBECOM)*, 2015, pp. 1–7.

[6] X. Yang, W. Jiang, and B. Vucetic, "A random beamforming technique for omnidirectional coverage in multiple-antenna systems," *IEEE Trans. Veh. Technol.*, vol. 62, no. 3, pp. 1420–1425, March 2013.

[7] M. Giordani, M. Mezzavilla, and M. Zorzi, "Initial access in 5G mm-wave cellular networks," *Submitted to IEEE Communications Magazine*, vol. abs/1602.07731, 2016. [Online]. Available: http://arxiv.org/abs/1602.07731

[8] G. Lee, Y. Sung, and J. Seo, "Randomly-directional beamforming in millimeter-wave multiuser miso downlink," *IEEE Transactions on Wireless Communications*, vol. 15, no. 2, pp. 1086–1100, Feb 2016.

[9] G. Lee, Y. Sung, and M. Kountouris, "On the performance of random beamforming in sparse millimeter wave channels," *IEEE J. Sel. Topics Signal Process.*, vol. PP, no. 99, pp. 1–1, 2016.

[10] J. Chung, C.-S. Hwang, K. Kim, and Y. K. Kim, "A random beamforming technique in MIMO systems exploiting multiuser diversity," *IEEE J. Sel. Areas Commun.*, vol. 21, no. 5, pp. 848–855, June 2003.

[11] A. Shahmansoori, G. E. Garcia, G. Destino, G. Seco-Granados, and H. Wymeersch, "5G position and orientation estimation through millimeter wave MIMO," in *Proc. IEEE Globecom Workshops,*, Dec 2015.

[12] V. Raghavan, J. Cezanne, S. Subramanian, A. Sampath, and O. Koymen, "Beamforming tradeoffs for initial UE discovery in millimeter-wave mimo systems," *IEEE J. Sel. Topics Signal Process.*, vol. 10, no. 3, pp. 543–559, April 2016.

[13] A. Guerra, F. Guidi, and D. Dardari, "Position and orientation error bound for wideband massive antenna arrays," in *2015 IEEE International Conf. on Commun. Workshop (ICCW)*, June 2015, pp. 853–858.

[14] T. Rappaport, E. Ben-Dor, J. Murdock, and Y. Qiao, "38 GHz and 60 GHz angle-dependent propagation for cellular peer-to-peer wireless commun." in *IEEE Intl Conf. on Commun.*, June 2012, pp. 4568–4573.

[15] S. Lin, K. B. Ng, H. Wong, K. M. Luk, S. S. Wong, and A. S. Y. Poon, "A 60GHz digitally controlled rf beamforming array in 65nm CMOS with off-chip antennas," in *Radio Frequency Integrated Circuits Symposium (RFIC), 2011 IEEE*, June 2011, pp. 1–4.

[16] A. S. Y. Poon and M. Taghivand, "Supporting and enabling circuits for antenna arrays in wireless communications," *Proceedings of the IEEE*, vol. 100, no. 7, pp. 2207–2218, July 2012.

[17] S. Kay, *Fundamentals of Statistical Signal Processing: Estimation theory*, ser. Fundamentals of Statistical Signal Process. Prentice-Hall, 1993.

[18] H. Deng and A. Sayeed, "Mm-wave MIMO channel modeling and user localization using sparse beamspace signatures," in *IEEE 15th Intl Workshop on Sig. Process. Adv. in Wireless Commun. (SPAWC), 2014*, June 2014, pp. 130–134.